Deciphering Bedaquiline and Clofazimine Resistance in Tuberculosis: An Evolutionary Medicine Approach

Lindsay Sonnenkalb[+,1], Joshua Carter[+,2], Andrea Spitaleri[5,6], Zamin Iqbal[7], Martin Hunt[7,8], Kerri Malone[7], Christian Utpatel[1], Daniela Maria Cirillo[5], Camilla Rodrigues[9], Kayzad S. Nilgiriwala[10], the CRyPTIC Consortium[11], Philip W. Fowler[&,8], Matthias Merker[&,1], Stefan Niemann[&,1,3,4]

Affiliations

[1]Molecular and Experimental Mycobacteriology, Research Center Borstel Leibniz Lung Center, Borstel Germany

[2]Medical Scientist Training Program, Stanford University, Stanford, USA

[3]National Reference Center, Research Center Borstel Leibniz Lung Center, Borstel Germany

[4]German Centre for Infection Research (DZIF), Partner site Hamburg-Lübeck-Borstel, Borstel, Germany

[5]Emerging Bacterial Pathogens Unit, Division of Immunology, Transplantation and Infectious Diseases, IRCCS San Raffaele Scientific Institute, Milan, Italy

[6]Center for Omics Sciences, IRCCS San Raffaele Scientific Institute, Milan, Italy

[7]European Bioinformatics Institute, Cambridge, UK.

[8]Experimental Medicine, Nuffield Department of Medicine, University of Oxford, UK

[9]Department of Microbiology, P. D. Hinduja National Hospital and Medical Research Centre, Mumbai, India

[10]The Foundation for Medical Research, Mumbai, India

[11]Comprehensive Resistance Prediction for Tuberculosis: an International Consortium. Author list in supplement.

[+]equally contributing first authors

[&]equally contributing last authors

*Corresponding author, email: sniemann@fz-borstel.de

Abstract

Bedaquiline (BDQ) and clofazimine (CFZ) are core drugs for treatment of multidrug resistant tuberculosis (MDR-TB), however, our understanding of the resistance mechanisms for these drugs is sparse which is hampering rapid molecular diagnostics. To address this, we employed a unique approach using experimental evolution, protein modelling, genome sequencing, and minimum inhibitory concentration data combined with genomes from a global strain collection of over 14,151 *Mycobacterium tuberculosis* complex isolates and an extensive literature review. Overall, 230 genomic variants causing elevated BDQ and/or CFZ MICs could be discerned, with 201 (87.4%) variants affecting the transcriptional repressor (Rv0678) of an efflux system (mmpS5-mmpL5). Structural modelling of Rv0678 suggests four major mechanisms that confer resistance: impairment of DNA binding, reduction in protein stability, disruption of protein dimerization, and alteration in affinity for its fatty acid ligand. These modelling and experimental techniques will improve personalized medicine in an impending drug resistant era.

Introduction

Multidrug-resistant (MDR: resistance to at least isoniazid [INH] and rifampicin [RMP]) Mycobacterium tuberculosis complex (Mtbc) strains represent a serious challenge for global tuberculosis (TB) control [1,2]. The World Health Organization (WHO) estimates that close to half a million people worldwide were infected in 2019 with an RMP-resistant (RR) Mtbc strain, of whom 78% were MDR [1].

Compared to patients with sensitive TB, treating MDR-TB treatment takes longer (years), the drugs are less effective and more toxic, and cure rates are low (about 60% globally) [1,3]. As a consequence, ineffective MDR-TB regimens in many high incidence settings have led to an expansion of drug resistant Mtbc strains. The WHO has recommended new treatment regimens for MDR-TB, including new and repurposed drugs such as bedaquiline (BDQ) and clofazimine (CFZ) [4–7]. Both drugs are now central to MDR-TB therapy, and are also part of the recently WHO-endorsed shorter, all-oral MDR-TB regimen [7,8].

Selection experiments have found resistance to BDQ and or CFZ as mediated by mutations in the genes *atpE*, *pepQ*, *Rv1979c* [9–11], and *Rv0678* - the latter of which seems to be the most clinically relevant and strains with BDQ associated mutations in *Rv0678* and *atpE* have been selected in multiple patients[12–17]. Rv0678 is a marR-like transcriptional regulator of the mmpS5-mmpL5 efflux pump with a canonical N-terminal winged helix-turn-helix (wHTH) DNA binding domain and a C-terminal helical dimerization domain. The Rv0678 protein forms a homodimer which binds to the promotor region of the mmpS5-mmpL5 operon [18–21]. This repression is reversed upon the conformational change of the Rv0678 molecule in the presence of a fatty acid ligand [20]. Importantly, Mtbc strains with mutations in *Rv0678* have been shown to confer resistance against both BDQ and CFZ [22,23], thus undermining the recently WHO-endorsed treatment guidelines [8]. Moreover, mutations in *Rv0678* are the most common resistance mechanism to CFZ and BDQ found in patient isolates today [16,17,24–29].

So far, mutations scattered across the full gene length of *Rv0678* (498bp) have been found to occur *in vitro* and in patients isolates leading to variable shifts in BDQ and CFZ minimum inhibitory concentrations (MICs) [13,29,30]. However, a comprehensive understanding of the associations between *Rv0678* mutations and their resulting phenotype, as well as their structural effects on the transcriptional repressor Rv0678, is lacking.

In this paper we present the results of an experimental model that evolves Mtbc strains under sub-lethal drug concentrations. Such a weak selection pressure has been shown to select for diverse pheno- and genotypes in other bacterial species and likely also reflects the physiological conditions in TB patients [31–33]. Recent studies indicate the inability of most drugs to diffuse into the granuloma at therapeutic levels, including CFZ and BDQ which strongly bind caseum macromolecules [34–38]. BDQ has further been shown to accumulate in cellular compartments of various types of macrophages (including neutrophils), but was unevenly distributed in intracellular bacteria [39,40]. Single resistant clones and total bacterial populations from consecutive cultivation passages were selected at clinically relevant drug concentrations, analyzed by whole genome sequencing (WGS), and compared with mutations identified in 14,151 patient isolates collected by the CRyPTIC consortium. Selected mutations were further investigated computationally for their putative effects on the Rv0678 protein structure and function, which provides a starting point for design of computational algorithms to predict drug resistance. The data generated provide a comprehensive resistance mutation catalogue for genotypic BDQ/CFZ drug susceptibility testing and will improve MDR-TB treatment design and likely outcomes for patients receiving a BDQ and/or CFZ containing therapies.

Results

Experimental evolution under sub-lethal drug concentrations

To better understand the resistance mechanisms of Mtbc strains against BDQ (which often includes correlated resistance to CFZ), we evolved Mtbc strains under sub-lethal drug concentrations. The experimental set-up was developed to allow for a high number of bacterial generations under a moderate drug selection pressure, thus increasing the mutation diversity compared to classical mutant selection experiments, i.e. exposing a culture at a late exponential phase to the critical drug concentrations (Figure S1). Our H37Rv laboratory strain (ATCC 27294) MIC was 0.25 mg/L for BDQ and 0.5 mg/L for CFZ, in high bacterial density liquid culture (10^7 CFU/mL inoculum) – we shall refer to these as the wild-type (WT) MICs. During five culture passages spread over 20 days, we exposed H37Rv to either BDQ or CFZ at one of four concentrations, ranging from one-half to one-sixteenth of the WT MIC (Figure S2), and selected colonies on solid media (7H11 plates) supplemented with 0.12 mg/L (1:2 MIC) and 0.25 mg/L (MIC) for BDQ and 0.25 mg/L (1:2 MIC) for CFZ. At passages 1, 3, and 5, single colonies as well as the whole bacterial

95 population were genotypically characterized, and single selected mutations were phenotypically defined
96 (elevated MIC) (Tables 1, S1).

97 Strikingly, exposure to BDQ or CFZ concentrations as low as one-eighth of the WT MIC over 20 days (12 to
98 19 generations) led to the selection and enrichment of significantly more resistant cells as compared to
99 growth in the absence of the drugs ($P=2.8 \times 10^{-10}$, and $P=2.4 \times 10^{-3}$, respectively, Figure S2). As expected,
100 there was less enrichment of resistant populations at early timepoints, e.g. after 4 days.

101 **Table 1: *In vitro* selected mutations conferring BDQ resistance.** Genotype of each variant was determined
102 by whole genome sequencing, and substitution annotated by coding position, "alternative allele" denotes
103 base pair change. Minimum inhibitory concentration (MIC) was determined by resazurin microtiter plate
104 assay and compared to wild type (WT) susceptible ancestor to describe MIC fold increase. The number of
105 times a mutation was independently selected was included under "# of clones". Finally, from which
106 experiment (BDQ or CFZ) the mutant was isolated from included as "isolate from".

Gene	Position	Substitu-tion	Type	Alt. allele	# of clones	BDQ MIC (mg/L)	BDQ MIC fold increase	CFZ MIC (mg/L)	CFZ MIC fold increase	Isolated from	Drug concentration of selection media (mg/L)
	WT ancestor					0.25-0.5		0.5-1			
Rv0678	778980	promotor	indel	-9 ins g	1	2	4-8	1	0-2	BDQ	0.12
Rv0678	779005	6fs	indel	16 del g	1	1	2-4	2	2-4	BDQ	0.12
Rv0678	779015	9fs	indel	26 del ag	1	2	4-8	NA	NA	BDQ	0.12
Rv0678	779029	14fs	indel	40 del c	1	2	4-8	2	2-4	BDQ	0.12
Rv0678	779038	17fs	indel	49 del a	1	2	4-8	2	2-4	CFZ	0.25
Rv0678	779051	21fs	indel	62 del a	1	2	4-8	1	0-2	BDQ	0.12
Rv0678	779060	G24V	SNP	T	3	2	4-8	2	2-4	CFZ	0.25
Rv0678	779062	G25S	SNP	A	1	2	4-8	NA	NA	BDQ	0.25
Rv0678	779078	30fs	indel	89 del g	1	2	4-8	2	2-4	CFZ	0.25

Rv0678	779101	R38*	SNP	T	4	2	4-8	2	2-4	CFZ	0.25
Rv0678	779102	R38P	SNP	C	1	1	2-4	2	2-4	CFZ	0.25
Rv0678	779108	L40S	SNP	C	1	1	2-4	2	2-4	CFZ	0.25
Rv0678	779109	40fs	indel	120 del g	1	1	2-4	2	2-4	CFZ	0.25
Rv0678	779117	L43P	SNP	C	5	1-2	2-8	2	2-4	BDQ/CFZ	0.12 / 0.25
Rv0678	779117	L43R	SNP	G	1	1	2-4	2	2-4	BDQ	0.12
Rv0678	779120	L44P	SNP	C	4	1	2-4	2	2-4	CFZ	0.25
Rv0678	779137	R50W	SNP	T	12	1	2-4	2	2-4	CFZ	0.25
Rv0678	779141	Q51R	SNP	G	2	2	4-8	4	4-8	CFZ	0.25
Rv0678	779149	E54*	SNP	T	1	2	4-8	2	2-4	CFZ	0.25
Rv0678	779152	E55*	SNP	T	1	1	2-4	2	2-4	CFZ	0.25
Rv0678	779159	A57E	SNP	A	1	2	4-8	2	2-4	CFZ	0.25
Rv0678	779174	A62D	SNP	A	1	2	4-8	2	2-4	CFZ	0.25
Rv0678	779176	S63G	SNP	G	5	2	4-8	2	2-4	CFZ	0.25
Rv0678	779181	64fs	indel	192 ins g	20	1-4	2-16	2-4	2-8	BDQ/CFZ	0.12 / 0.25
Rv0678	779182	65fs	indel	193 del g	12	1-2	2-8	2-4	2-8	BDQ/CFZ	0.12 & 0.25 / 0.25
Rv0678	779186	G66E	SNP	A	1	2	4-8	1	0-2	BDQ	0.12
Rv0678	779191	S68G	SNP	G	9	1-2	2-8	2	2-4	BDQ/CFZ	0.12 / 0.25
Rv0678	779203	R72W	SNP	T	2	1-2	2-8	2	2-4	CFZ	0.25
Rv0678	779204	R72L	SNP	T	2	2-4	4-16	4-6	4-12	BDQ	0.12
Rv0678	779210	L74P	SNP	C	8	1-2	2-8	2-4	2-8	BDQ/CFZ	0.12 / 0.25
Rv0678	779217	76fs	indel	228 ins t	1	2	4-8	NA	NA	BDQ	0.12
Rv0678	779224	F79V	SNP	G	1	1	2-4	2	2-4	CFZ	0.25
Rv0678	779225	F79C	SNP	G	2	1	2-4	2	2-4	BDQ	0.12
Rv0678	779240	A84V	SNP	T	2	1-2	2-8	1-2	0-4	BDQ	0.12
Rv0678	779252	88fs	indel	263 ins t	1	2	4-8	1	0-2	BDQ	0.12
Rv0678	779263	92fs	indel	274 ins a	3	1	2-4	2	2-4	CFZ	0.25
Rv0678	779270	94fs	indel	281 del g	1	2	4-8	2	2-4	CFZ	0.25
Rv0678	779280	97fs	indel	291 ins a	2	2	4-8	2	2-4	CFZ	0.25
Rv0678	779281	98fs	indel	292 del g	1	2	4-8	2	2-4	BDQ	0.12
Rv0678	779285	A99V	SNP	T	16	1-2	2-8	1-2	0-4	BDQ/CFZ	0.12 / 0.25
Rv0678	779293	A102T	SNP	A	4	1-4	2-16	2-4	2-8	BDQ	0.12

Rv0678	779296	G103R	SNP	C	1	1	2-4	2	2-4	BDQ	0.12
Rv0678	779330	L114P	SNP	C	1	2	4-8	2	2-4	CFZ	0.25
Rv0678	779332	Q115*	SNP	T	1	2	4-8	2	2-4	BDQ	0.12
Rv0678	779342	A118D	SNP	C	1	1	2-4	2	2-4	CFZ	0.25
Rv0678	779349	120fs	indel	360 del g	7	1-4	2-16	2-4	2-8	BDQ/CFZ	0.12 / 0.25
Rv0678	779351	G121E	SNP	A	3	2	4-8	2-4	2-8	CFZ	0.25
Rv0678	779354	L122P	SNP	C	1	2	4-8	2	2-4	CFZ	0.25
Rv0678	779363	125fs	indel	374 del t	1	2	4-8	2	2-4	BDQ	0.12
Rv0678	779363	L125P	SNP	C	1	2	4-8	2	2-4	CFZ	0.25
Rv0678	779384	R132P	SNP	C	1	2	4-8	2	2-4	CFZ	0.25
Rv0678	779392	R135W	SNP	T	1	2	4-8	2	2-4	BDQ	0.12
Rv0678	779396	L136P	SNP	C	2	2	4-8	2-4	2-8	BDQ	0.12
Rv0678	779406	139fs	indel	417 ins CGGG ATCTG TTGGC ATATA T	2	1-2	2-8	2	2-4	BDQ	0.12
Rv0678	779414	142fs	indel	425 del t	1	2	4-8	2	2-4	CFZ	0.25
Rv0678	779415	142fs	indel	426 ins TTGGC ATA	1	2	4-8	NA	NA	BDQ	0.12
Rv0678	779424	Y145*	SNP	G	6	1-2	2-8	2	2-4	BDQ/CFZ	0.12 & 0.25 / 0.25
Rv0678	779440	S151P	SNP	C	1	2	4-8	2	2-4	BDQ	0.12
Rv0678	779450	L154P	SNP	C	2	2	4-8	2	2-4	CFZ	0.25
Rv0678	779454	155fs	indel	465 ins c	2	1-2	2-8	2	2-4	CFZ	0.25
Rv0678	779455	R156*	SNP	T	3	2	4-8	2	2-4	BDQ/CFZ	0.12 & 0.25 / 0.25
Rv0678	-	-	inversion	-	3	2	4-8	2	2-4	BDQ	0.12
Rv1305	1461127	D28G	SNP	G	1	≥10	20	NA	NA	BDQ	0.25
Rv1305	1461127	D28V	SNP	T	3	≥8	16	NA	NA	BDQ	0.25
Rv1305	1461227	E61D	SNP	C	5	2-≥10	4-40	1	0-2	BDQ	0.25
Rv1305	1461227	E61D	SNP	T	2	≥10	20	1-2	0-4	BDQ	0.12 & 0.25
Rv1305	1461231	A63P	SNP	C	7	≥10	20	1-2	0-4	BDQ	0.25

Alt- alternative, BDQ- bedaquiline, CFZ- clofazimine, del- deletion, fs- frameshift, ins- insertion, MIC- minimum inhibitory concentration, NA- not available, SNP- single nucleotide polymorphism, *-stop codon

Phenotypic and genotypic characterization of BDQ resistant mutants

In total, we randomly selected 270 single colonies from BDQ- and CFZ-supplemented agar plates that had been inoculated with samples from passages 1 (4 days), 3 (12 days), and 5 (20 days), of two independent experiments (Figure S1). In total, 203/270 mutants were successfully pheno- and genotyped (67 were excluded due to DNA library preparation issues or inadequate growth). The single colonies were sub-cultured and the MICs for BDQ and CFZ were determined for each clone using broth microtiter dilution. All clones exhibited an elevated MIC at least 2-fold higher than the WT drug susceptible ancestor and we identified in total 61 unique variants with one mutation in the *Rv0678* gene per clone. We additionally selected five unique mutations in the *atpE* (*Rv1305*) gene (Table 1).

Clones which harbored a mutation in *Rv0678* had a 2-4-fold MIC increase for BDQ, whereas mutations in *atpE*, exhibited 4 to over 10 times the MIC of the WT strain (Table 1). For 12 randomly selected clones with seven different variants we verified the results obtained in broth microtiter dilution plates using a Mycobacterium growth indicator tube (MGIT) assay. These experiments showed comparable MICs of the mutant clones with those obtained from the previous method (Table S2).

The 61 unique mutations in *Rv0678* affected 54 different codons (Table 1), out of which 21 (34%) were frameshift (fs) mutations, 34 (56%) had one non-synonymous SNP, and 6 (10%) a premature inserted stop codon. The mutations were scattered over the entire sequence of *Rv0678* and no dominant cluster could be identified (Figure 1A). However, the four mutations which were most frequently observed were: 192 ins g (64fs), A99V, 193 del g (65fs), and R50W; these mutations were detected in 19, 17, 13, and 12 single selected clones, respectively (Table 1). Notably, nucleotides 192-198 were also identified as a hotspot for frameshifting variation in a prior review, potentially due to the homopolymeric nature of this region[41].

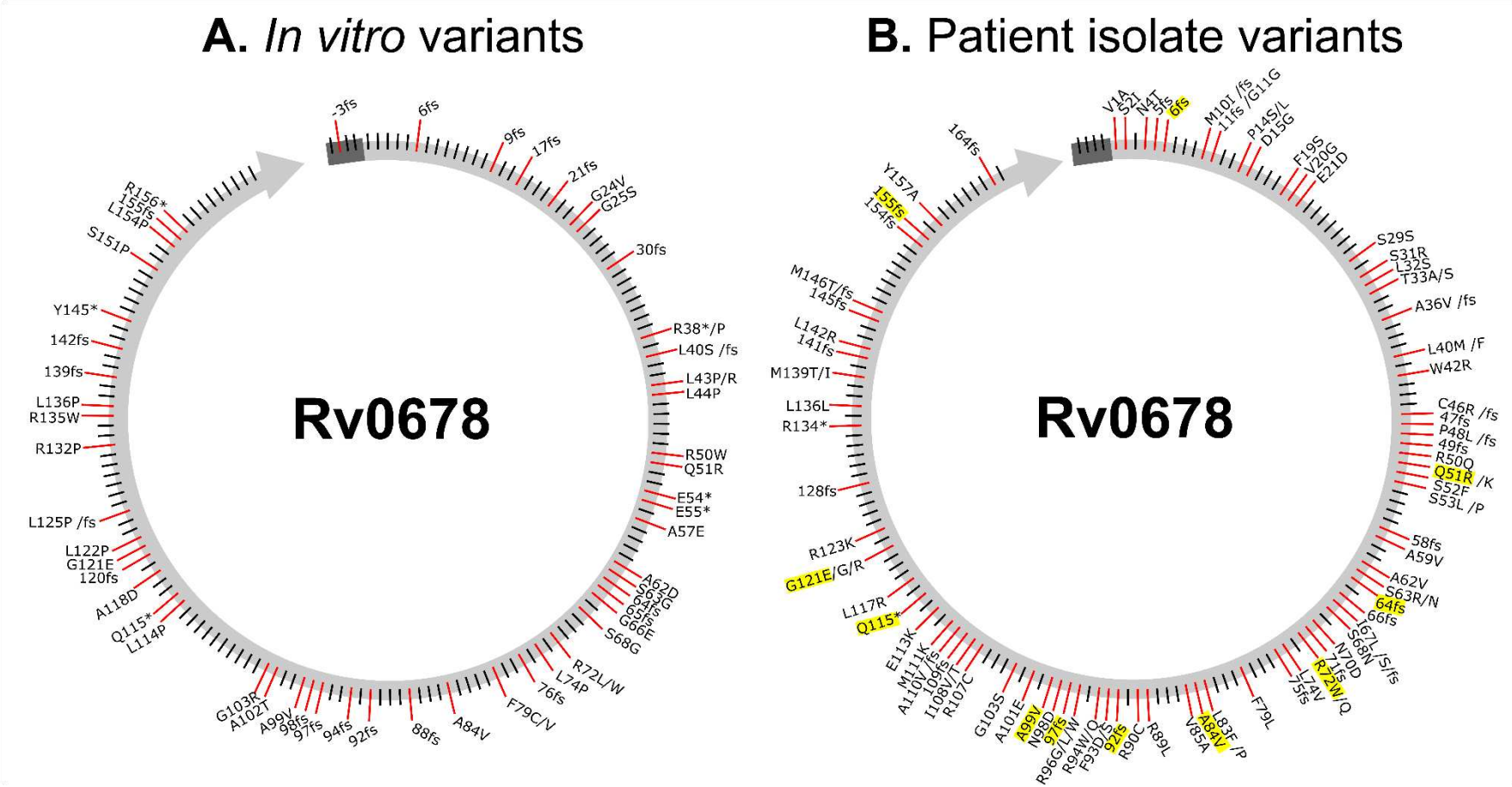

Figure 1: BDQ resistance associated variants mapped in *Rv0678* gene. Resistance associated mutations detected within patient dataset and *in vitro* selection were designated along Rv0678 gene at corresponding coding positions by non-synonymous single nucleotide polymorphisms, and by a protein disrupting mutation such as a stop codon insertion (*) or frameshift (fs) mutations. Data sets divided by (A) mutations which were selected in *in vitro* experiments with elevated minimum inhibitory concentrations verified to bedaquiline, and (B) mutations which were detected in patient isolates either collected by CRyPTIC or described in published literature. Overlapping mutations in observed in both patients and *in vitro* are highlighted in yellow.

As mentioned before, no mutant clone had more than one resistance mediating variant in *Rv0678* or *atpE*, however, 38 mutants harbored a second mutation in one of 14 genes that have not been previously proposed to be associated with resistance against BDQ and/or CFZ (Table S3). The most common mutation found in addition to *Rv0678* mutations was R119H in *Rv1890c* – this gene codes for a conserved hypothetical protein [42], and the mutation was selected 11 times along with six different resistance mutations. The second most common co-selected mutation was *130R in *Rv1871c* (a conserved hypothetical membrane protein [43]) that was selected seven times along with four different resistance mutations. Other secondary mutations occurred in genes which were involved in cell wall synthesis, information pathways, metabolism/respiration, protein regulation, or lipid metabolism (Table S3).

In addition to single colony sequencing, we also employed a more unbiased approach based on population sequencing of all the mutant colonies on a given plate, in order to elucidate all possible variants. On average the genome wide coverage for a total of 81 samples was 308±50. We then reported mutations if the position was covered by at least one read in both forward and reverse orientations and there were two reads with a phred score over 20. This identified 45 additional mutations in *Rv0678* and one in *atpE* (A63T), as well as four mutations in *pepQ* (*Rv2535c*; F97V, G96G, V92G, A87G) (Table S1). As in the single colony analysis, we found the following mutations dominating in different independent evolutionary experiments and selected across different drug concentrations: *Rv0678* 192 ins g (64fs), A99V, R50W, and L43P.

Resistance caused by huge inversion interruption in Rv0678

Three mutants with elevated BDQ (2 mg/L) and CFZ (2 mg/L) MICs but lacking mutations in the BDQ/CFZ resistance associated genes were further subjected to long read sequencing with the PacBio Sequel II system. A *de novo* assembly employing the PacBio SMRT® Link software resulted in one closed Mtbc genome, and two assemblies with 1 and 4 four contiguous sequences (contigs), respectively. All assemblies covered more than 99.9% of the H37Rv reference genome (NC_000962.3). All three assemblies showed a large-scale sequence re-arrangement with the borders at position 779,073 (Rv0678 coding sequence) and 3,552,584 (intergenic region), flanked by a transposase open reading frame (IS*6110*). A 2.5Mb fragment was inverted and thus split the *Rv0678* gene into halves (Figure 2), which was not detected by a classical reference mapping approach and revealed a further interesting resistance mechanism. We scanned all BDQ resistant samples in the CRyPTIC strain collection for similar events using

local assembly with ARIBA [44]. In one isolate we assembled one contig which clearly represented a similar inversion disrupting *Rv0678*, but since the depth of support was just 1 read (mean, across the contig) and this was Illumina (short read) data, we considered this only circumstantial evidence.

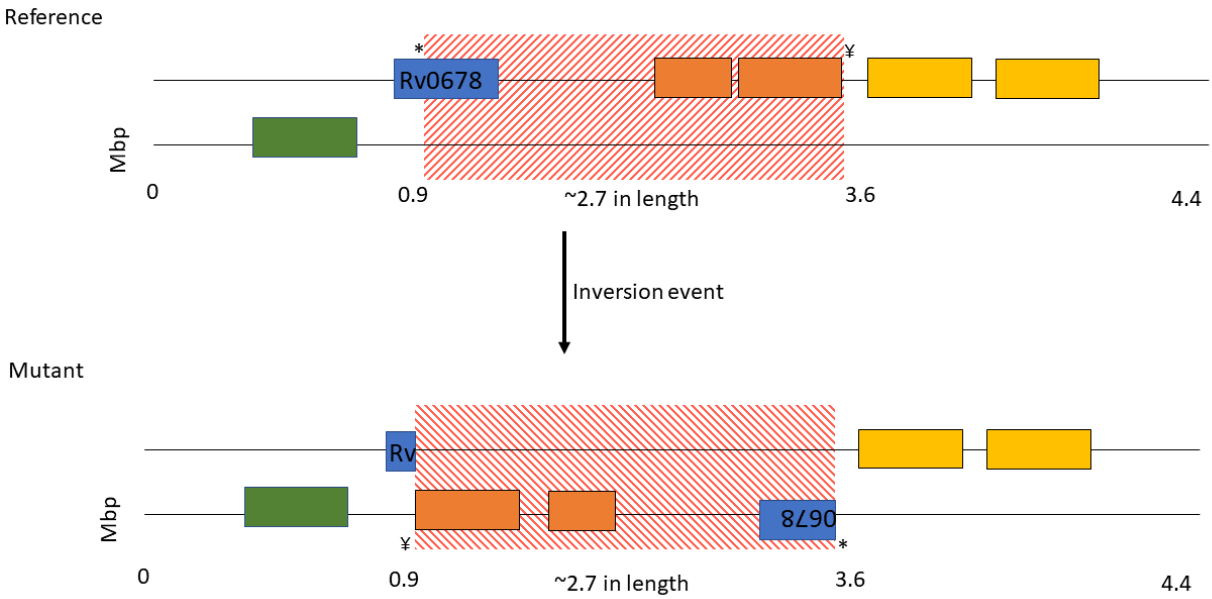

Figure 2: Large scale gene rearrangement in Rv0678 gene. *De novo* assembly using PacBio SMRT® Link software indicated a 2.7 Mb inversion (red) impacting *Rv0678* (blue), at positions 779,073 coding sequence (amino acid 34 in Rv0678) and 3,552,584 intergenic region; flanked by transposase related genes (orange and yellow).

Mutations associated with bedaquiline and clofazimine resistance in clinical isolates

Next, we aimed to comprehensively describe the BDQ and CFZ resistant variants occurring in patients, to develop a catalogue of known resistance variants. We searched the literature for patient reports describing BDQ resistance during MDR-TB therapy and analyzed pheno- and genotypes of 14,151 clinical Mtbc strains collected by the CRyPTIC consortium (Table S4). In this patient dataset, we identified 98 mutations throughout *Rv0678*, 71 of which were not previously described in patients (Table 2). In addition, seven variants in *Rv0678* harbored mutations found in different lineages (Table S4), pointing to convergent evolution at these sites. Eleven mutations from the patient-derived set were also shared with our *in vitro* derived datasets (selected variants and population sequencing) (Figure 1B & 3A).

Table 2: *Rv0678* mutations detected in patients (published literature and CRyPTIC collection). Reference catalog of *Rv0678* mutations which have been described in previously published patient isolates or collected by the Comprehensive Resistance Prediction for Tuberculosis an International Consortium (CRyPTIC) partners. Additionally, alternative (Alt.) allele information included, describes the variants at the base pair position. Variants included in list if presented a borderline or resistant phenotype to at least bedaquiline (BDQ)MIC determined by different drug susceptibility testing (DST) techniques depending on the study, abbreviated as: [A] BD-MGIT™, [B] UKMYC5/UKMYC6 plates, [C] Alamar blue/resazurin assay, [D] 7H10 plates, [E] 7H11 plates

Phenotype interpretation was based off of: [A] 1mg/L BDQ/CFZ[45]; [B] 0.12-0.25mg/L BDQ/CFZ[46], [C] defined by study authors, [D] 0.5mg/L BDQ[47]/CFZ[48], [E] 0.25 mg/L BDQ[45] -CFZ determined by study authors

Gene	Substitu-tion	Alt Allele	Type	BDQ MIC (mg/L)	CFZ MIC (mg/L)	Phenotype interpretation BDQ- R, B, S	Phenotype interpretation CFZ- R, B, S	DST Method	Author
Rv0678	V1A	c	SNP	6.4/0.5	>4/NA	R/B	R	[A]	[24,25]
Rv0678	S2I	t	SNP	0.73	4	R	R	[C]	[28]
Rv0678	N4T	acc	SNP	0.06-0.12	0.12	S/B	B	[B]	CRyPTIC
Rv0678	5fs	15 del c	indel	0.5	0.25	R	R	[B]	CRyPTIC
Rv0678	6fs	18 del gg	indel	0.5	NA	R	NA	[E]	[49]
Rv0678	6fs	16 del gg	indel	0.5	NA	R	NA		[50]
Rv0678	10fs	28 del t	indel	0.12	≤0.06	B	S	[B]	CRyPTIC
Rv0678	10fs	29 del t	indel	0.25	0.12	R	B	[B]	CRyPTIC
Rv0678	M10I	atc	SNP	0.12	NA	B	NA	[B]	CRyPTIC
Rv0678	11fs	32 del g	indel	0.25	NA	R	NA	[E]	[51]
Rv0678	G11G	t	SNP	0.5-2.0	NA	R	NA	[C]	[52]
Rv0678	P14S	tcc	SNP	0.25	0.5	R	R	[B]	CRyPTIC
Rv0678	P14L	ctc	SNP	0.12	≤0.06	B	S	[B]	CRyPTIC
Rv0678	D15G	NA	SNP	0.25	NA	R	NA	[B]	CRyPTIC
Rv0678	F19S	tcc	SNP	0.5	NA	R	NA	[B]	CRyPTIC
Rv0678	V20G	NA	SNP	0.25/2/0.25/0.25	NA/2/NA/4	R/B	R	[E]/[A]/[A]/[E]	[53,53,54,29]
Rv0678	V20A	gcc	SNP	0.12	0.12	B	B	[B]	CRyPTIC
Rv0678	E21D	c	SNP	0.5-1.0	NA	R	NA	[C]	[52]
Rv0678	S29S	tct	SNP	0.12	0.12	B	B	[B]	CRyPTIC
Rv0678	S31R	c	SNP	0.5	NA	R	NA	[C]	[52]

Rv0678	L32S	tcg	SNP	0.12	0.12	B	B	[B]	CRyPTIC
Rv0678	T33A	g	SNP	0.5	2	R	R	[C]	[23]
Rv0678	T33S	g	SNP	2	NA	R	NA	[C]	[52]
Rv0678	A36V	t	SNP	0.5	4	R	R	[C]	[23]
Rv0678	36fs	107 ins g	indel	0.5	0.25	R	R	[B]	CRyPTIC
Rv0678	L40M	atg	SNP	0.5	NA	R	NA	[B]	CRyPTIC
Rv0678	L40F	ttc	SNP	0.5	NA	R	R	[B]	CRyPTIC
Rv0678	W42R	cgg	SNP	0.25/0.12	0.25/2	R/B	R	[B]/[D]	CRyPTIC, [14]
Rv0678	46fs	136 ins g	indel	1	NA	R	NA	[E]	[54]
Rv0678	46fs	137 ins g	indel	0.25	1	R	R	[B]	CRyPTIC
Rv0678	46fs	138 ins g	indel	0.25/0.25/2/>1/1	0.25/NA/4/NA/NA	R	R	[B]/[E]/[A]/[E]/[E]	CRyPTIC, [53],[53],[12],[54]
Rv0678	46fs	138 ins ga	indel	>1.0	NA	R	NA	[E]	[15]
Rv0678	C46R	cgt	SNP	0.25	NA	R	NA	[B]	CRyPTIC
Rv0678	47fs	139 ins g	indel	0.25	NA	R	NA	[E]	[51]
Rv0678	47fs	140 ins g	indel	0.25	NA	R	NA	[E]	[49]
Rv0678	47fs	141 ins c	indel	0.06-0.25/0.5/4/0.5	0.06-1/NA/4/NA	S-R	S-R	[B]/ [E]/ [A]/[E]	CRyPTIC, [53],[53],[29]
Rv0678	48fs	144 ins c	indel	0.25	NA	R	NA	[E]	[51]
Rv0678	P48L	NA	SNP	0.25-0.5	NA	R	B	[B]	CRyPTIC
Rv0678	E49fs	NA	indel	0.03-0.25	0.25-2	R	R	[E]	[29]
Rv0678	R50Q	NA	SNP	0.25	NA	R	NA	[B]	CRyPTIC
Rv0678	Q51K	NA	SNP	0.25	1	R	R	[B]	CRyPTIC
Rv0678	Q51R	NA	SNP	0.3	1	R	R	[B]	CRyPTIC
Rv0678	S52F	NA	SNP	0.48	NA	R	NA	[D]	[14]
Rv0678	S53L	NA	SNP	0.25-0.4	2	R	R	[C]	[28]
Rv0678	S53P	NA	SNP	0.5	2-4	R	R	[C]	[28]
Rv0678	58fs	172 ins IS6110	indel	0.5	1	R	R	[C]	[23]
Rv0678	A59V	NA	SNP	0.48	NA	R	NA	[D]	[14]
Rv0678	A62V	NA	SNP	0.48	NA	R	NA	[D]	[14]
Rv0678	A62T	acc	SNP	0.12	0.5	B	R	[B]	CRyPTIC
Rv0678	S63R	a	SNP	0.5	1.25	R	R	[C]	[22]
Rv0678	S63N	a	SNP	0.25	NA	R	NA	[C]	[55]

Rv0678	64fs	192 ins g	indel	0.03-0.25/0.5/4	0.12/NA/4	S-R	R	[B]/[E]/[A]	CRyPTIC, [53],[53]
Rv0678	64fs	192 ins c	indel	>1.0	NA	R	NA	[E]	[12]
Rv0678	66fs	198 ins g	indel	0.24-1	NA	R	NA	[D]	[14]
Rv0678	I67L	ctc	SNP	0.5	0.12	R	B	[B]	CRyPTIC
Rv0678	I67S	agc	SNP	0.5	0.25	R	R	[B]	CRyPTIC
Rv0678	S68N	aac	SNP	0.5	2	R	R	[B]	CRyPTIC
Rv0678	N70D	gat	SNP	0.25	NA	R	NA	[B]	CRyPTIC
Rv0678	71fs	212 del c	indel	0.5	1	R	R	[C]	[23]
Rv0678	R72W	NA	SNP	0.06-0.25	≤0.06->4	S-R	S-R	[B]	CRyPTIC
Rv0678	R72Q	a	SNP	0.757	2.77	R	R	[C]	[56]
Rv0678	L74V	gtg	SNP	0.25	0.12	R	B	[B]	CRyPTIC
Rv0678	75fs	224 ins a	indel	0.24	NA	R	NA	[D]	[14]
Rv0678	F79L	tta	SNP	0.12	0.12	B	B	[B]	CRyPTIC
Rv0678	L83F	NA	SNP	0.5	NA	R	NA	[B]	CRyPTIC
Rv0678	L83P	c	SNP	0.25	1	R	R	[B]	CRyPTIC
Rv0678	A84V	t	SNP	0.06	≤0.06	S/R	S/R	[B]	CRyPTIC
Rv0678	V85A	gcc	SNP	0.25/0.12	0.25	R/B	R	[B]/[E]	CRyPTIC, [51]
Rv0678	R89L	t	SNP	0.12	0.12	B	B	[B]	CRyPTIC
Rv0678	R90C	NA	SNP	0.3	0.16			[B]	CRyPTIC
Rv0678	92fs	274 ins a	indel	0.25/1	0.5/NA	R	NA	[B]/[D]	CRyPTIC, [14]
Rv0678	F93D	NA	SNP	0.25	NA	R	NA	[E]	[54]
Rv0678	F93S	NA	SNP	0.25	1	R	R	[E]	[29]
Rv0678	R94W	NA	SNP	2	4	R	R	[A]	[17]
Rv0678	R96W	NA	SNP	0.25	NA	R	NA		[50]
Rv0678	R96G	ggg	SNP	0.25	0.25	R	R	[B]	CRyPTIC
Rv0678	R96L	ctg	SNP	0.25	NA	R	NA	[B]	CRyPTIC
Rv0678	97fs	291 del c	indel	0.25	NA	R	NA	[E]	[51]
Rv0678	N98D	gac	SNP	0.25	≤0.06-0.12/NA/0.75-1/NA	R/S	S-R	[B]/[C]/[A]/[C]	CRyPTIC, [52], [30], [55]
Rv0678	A99V	t	SNP	0.25	NA	R	NA	[E]	[51]
Rv0678	A101E	gag	SNP	0.25	0.12	R	B	[B]	CRyPTIC
Rv0678	G103S	agc	SNP	0.03-0.12	0.5	B	R	[B]	CRyPTIC
Rv0678	R107C	NA	SNP	0.25	NA	R	NA	[B]	CRyPTIC

Rv0678	I108T	NA	SNP	0.25	0.25	R	B	[B]	CRyPTIC
Rv0678	I108V	gtc	SNP	0.12	0.25	B	R	[B]	CRyPTIC
Rv0678	109fs	325 ins g	indel	1	NA			[C]	CRyPTIC
Rv0678	A110V		SNP	0.5	0.5	B	R	[A]	[30]
Rv0678	110fs	329 del t	indel	0.12	≤0.06	B	S	[B]	CRyPTIC
Rv0678	M111K	NA	SNP	0.25	NA	R	NA		[50]
Rv0678	E113K	aaa	SNP	0.25	0.25	R	R	[B]	CRyPTIC
Rv0678	Q115*	tag	SNP	0.12	0.25	B	R	[B]	CRyPTIC
Rv0678	L117R	cgg	SNP	0.015-0.25/1.5	0.06-0.12/4.16	S-R	S-R	[B][C]	CRyPTIC, [28]
Rv0678	G121E	a	SNP	0.25	NA	R	R	[E]	[51]
Rv0678	G121R	agg	SNP	0.5/0.75	NA/2	R/B	R	[B]	CRyPTIC
Rv0678	G121G	gga	SNP	0.25	0.12	R	B	[B]	CRyPTIC
Rv0678	R123K	a	SNP	1	NA	R	NA	[C]	[52]
Rv0678	128fs	382 del t	indel	≤0.015	≤0.06	B	S	[B]	CRyPTIC
Rv0678	R134*	t	SNP	0.5	1.25	R	R	[C]	[22]
Rv0678	L136L	cta	SNP	0.12	NA	B	NA	[B]	CRyPTIC
Rv0678	M139T	NA	SNP	0.25	NA	R	NA	[E]	[49]
Rv0678	M139I	ata	SNP	0.25	0.25	R	R	[B]	CRyPTIC
Rv0678	141fs	421 ins g	indel	0.25	NA	R	NA	[E]	[51]
Rv0678	L142R	NA	SNP	0.25-1.0	NA	R	NA	[E]	[51]
Rv0678	145fs	435 del t	indel	0.25	NA	R	NA	[E]	[51]
Rv0678	146fs	438 ins t	indel	0.25	0.5			[E]	[54], [29]
Rv0678	M146T	acg	SNP	0.25-0.8	1.2	S-R	S-R	[B]/[C]/[A]	CRyPTIC, [28]
Rv0678	154fs	461 del t	indel	0.12	0.5	B	R	[B]	CRyPTIC
Rv0678	155fs	464 ins gc	indel	0.5	1			[B]	CRyPTIC
Rv0678	155fs	465 ins c	indel	0.12/1-2	0.25/2	B/R	R	[B]/[C]	CRyPTIC/ this study
Rv0678	Y157A		SNP	0.125	2	B	R	[C]	[57]
Rv0678	164fs	492 ins ga	indel	0.25	NA			[B]	CRyPTIC

Alt- alternative, BDQ- bedaquiline, CFZ- clofazimine, DST- drug susceptibility testing, del- deletion, fs- frameshift, ins- insertion, MIC- minimum inhibitory concentration, NA- not available, SNP- single nucleotide polymorphism, **-stop codon

196

197 Wild-type isolates presented an MIC95 of 0.12 mg/L BDQ/CFZ in the UKMYC5/6 plates[58]. Therefore, the
198 patient isolates in the study were catalogued as >0.12 mg/L BDQ/CFZ resistant, <0.12 susceptible, and
199 =0.12 borderline. The CRyPTIC dataset contained 178 patient isolates with a single *Rv0678* variant, 52 of
200 which were classified as BDQ resistant (27 cross-resistant with CFZ), 32 with borderline BDQ resistance,
201 and 94 BDQ susceptible (Table S4). To better explain this high number of BDQ susceptible strains with
202 *Rv0678* mutations we looked for additional mutations in the efflux pump genes *mmpL5* and *mmpS5*, as it
203 has been postulated that variants in these genes may reduce or abrogate acquired resistance [59]. However,
204 we found that 64/94 (68%) of susceptible isolates harboring *Rv0678* mutations had WT *mmpL5/mmpS5*
205 genes (Table S4). Likely functional/inactivating mutations in *mmpL5* (19/19 isolates with frameshifts and
206 3/5 with missense) were associated with susceptibility while synonymous mutations appeared
207 uncorrelated with susceptibility (7/18 isolates susceptible).

208 Plotting all 147 resistance and borderline resistance-associated *Rv0678* mutations on the gene sequence
209 (Figure 1), reveals that they occur throughout the entire length of the gene with no single hot spot region.
210 However, there are several regions where mutations are more likely to occur, i.e. codons 46-53 and 62-
211 68 (Figure 3B).

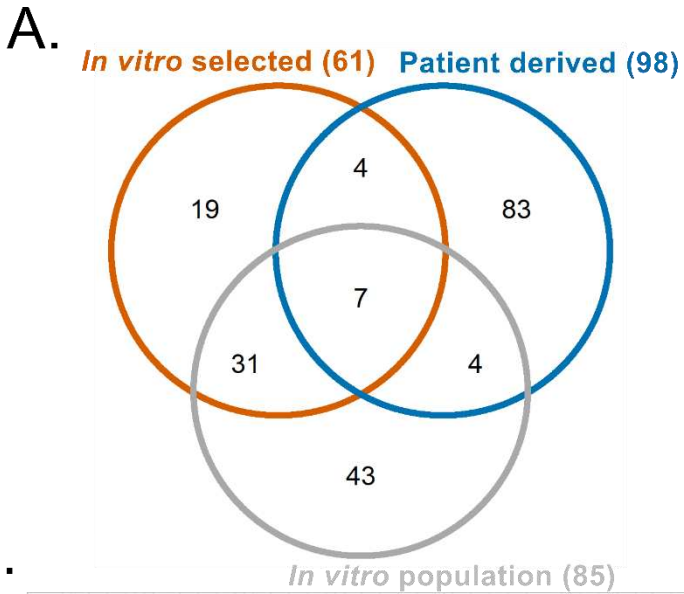
A.
In vitro selected (61)
Patient derived (98)
In vitro population (85)
19
4
83
7
31
4
43

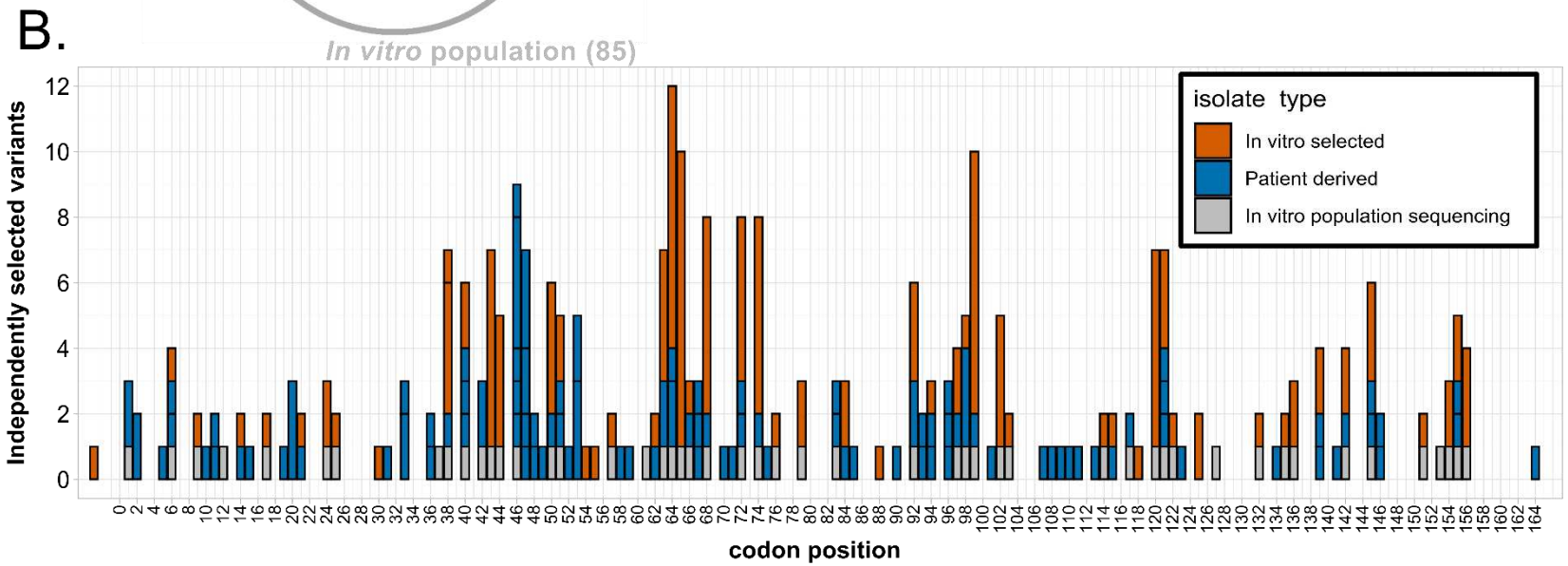
B.
Independently selected variants
codon position
isolate type
In vitro selected
Patient derived
In vitro population sequencing

212

Figure 3: Mutations and coding position overlap throughout *Rv0678, in vitro* and patient datasets. Overlapping mutations which conferred BDQ resistance were compared between three datasets: *in vitro* selected mutants (Table 1), *in vitro* population sequencing (Table S1), and patient derived variants (Table 2). (A) Venn diagram describes number overlapping mutations in the three datasets, all mutations must have the same SNP or a deletion/insertion at same coding position to overlap. (B) Data represents number of mutants selected at given coding position for *in vitro* selected (orange) and patient derived variants (blue), indicated with gray box if detected in *in vitro* population sequencing.

Next, we searched the CRyPTIC dataset for resistance conferring mutations (BDQ MIC >0.12 mg/L) in *atpE*, *pepQ* (*Rv2535c*) and *Rv1979c*. After filtering out phylogenetic SNPs and strains with preexisting *Rv0678* mutations, we found 35 isolates with an MIC >0.12 mg/L for BDQ harboring *Rv1979c* mutations and only 3 isolates with mutations in *atpE* [60]. There were no BDQ resistant isolates with *pepQ* mutations, but 19 strains had borderline BDQ resistance with an MIC of 0.12 mg/L. In total, we defined four *Rv1979c*-mediated resistant mutations, and 7 possible borderline-resistance conferring mutations in *pepQ* (*Rv2535c*).

Finally, after an in-depth literature search including *in vitro*, *in vivo*, and patient derived strains, we complied a comprehensive catalogue of variants in BDQ resistance associated genes (Table S5). Due to insufficient data for BDQ and CFZ critical concentration determination for many phenotypic assays, and the high overlap of MIC distributions between WT and mutant clones, resistance interpretation of mutations was based on the ascribed phenotype in each publication or by WHO critical concentration when available.

Structural variation in Rv0678

For better mechanistic understanding of how *Rv0678* mutations result in BDQ/CFZ resistance, we mapped missense mutations from our catalogue to the previously determined Rv0678 crystal structure (107 mutations mapped to resolved structure positions PDB ID 4NB5, Table S5) [20]. As mutations in different parts of the protein structure are likely to have different effects, we investigated four different mechanisms for conferring resistance: reducing folded protein/protein stability, impairing DNA binding, altering protein dimerization, and reducing affinity for the fatty acid ligand of Rv0678.

The numerous introductions of premature stop codons and frameshift mutations reported here and elsewhere suggest loss of functional Rv0678 protein is a common mechanism of resistance[22,41,51]. Consistent with this, if we compare the missense *Rv0678* mutations in resistant isolates with those in susceptible isolates, we find the former are more commonly predicted to destabilize the Rv0678 wHTH domain required for DNA binding (destabilization defined as $\Delta\Delta G <= -1$ kcal/mol as measured by mCSM protein stability, 34/38 R, 5/10 S, OR 7.96, Fisher exact p=0.012), suggesting that disruption of protein stability is also a resistance mechanism. These findings are also compatible with the observation that missense mutations from resistant isolates are predicted to have a more deleterious effect by SNAP2 score compared with those from susceptible isolates (Wilcoxon p=0.018) [61].

To understand how mutations may impact DNA binding, we structurally aligned the wHTH DNA binding domain of Rv0678 to several other Mtbc marR-family transcriptional regulators whose DNA-bound structures have been determined (Figure 4B, S3; average RMSD 0.81 Å)[62]. We found that mutations clustering in regions 62-68 and 88-92 correlate with the recognition α-helix and conserved DxR motif respectively, which directly contact the DNA and have previously been shown to critical for the binding affinity of other marR-family regulators (Figure 4B)[62,63]. However, further experimental verification of these mutations' effects on DNA binding is required.

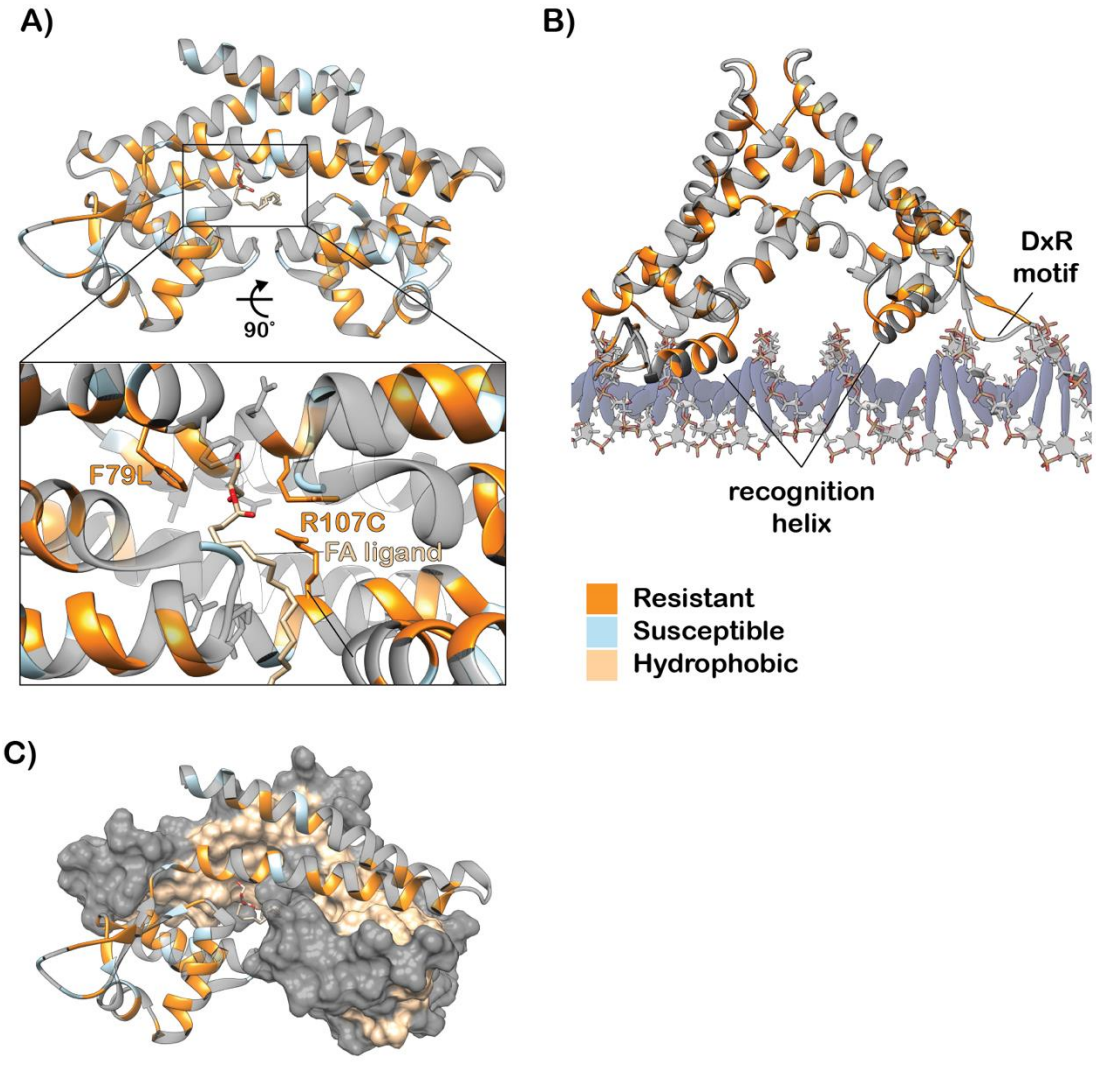

Figure 4: Structural mechanisms of BDQ resistance. (A) Rv0678 dimer with resistant (orange) and susceptible (blue) mutations shown. Pullout highlights the resistant mutations in the ligand binding

pocket. (B) Rv0678 dimer modeled onto DNA. Conserved MarR-family DNA binding elements are noted. (C) Resistant mutations occur across the hydrophobic dimerization domain.

We also investigated the possibility that mutations alter the protein-protein interactions of the Rv0678 dimer. Mutations associated with resistance are enriched at the dimer interface (27/29 interface mutations R), suggesting they may impact dimer formation and/or stability (Figure 4C). However, computational prediction of interface mutations' effects on non-DNA bound dimer stability revealed no significant difference in destabilization as defined by mCSM PPI ΔΔG <= -1 kcal/mol (16/27 R, 1/2 S). Interpretation of the DNA-bound dimer interface was not feasible due to the significant conformational rearrangement of the dimer alpha-helices upon DNA binding. Finally, all isolates where an amino acid that contacts the fatty acid ligand 2-stearoylglycerol was mutated were resistant, suggesting that disrupting the binding of the ligand confers resistance, possibly through perturbing non-DNA bound homodimer formation (Figure 4A).

Molecular dynamics simulations

Rv0678 must also undergo a conformational rearrangement to bind DNA which is not captured by the static structures in the previous section. Therefore, we employed molecular dynamics simulations to understand how particular mutations in the "hinge" region (connecting the DNA binding and dimerization domains) might disrupt this motion and lead to resistance. To do this, we performed 100ns simulations on the WT Rv0678 homodimer as well as Rv0678 homodimers containing either L40F and A101E mutations (which are associated with resistance but do not clearly interact with the DNA or disrupt protein folding) or the L40V mutation (consistently phenotypically susceptible). These simulations revealed that mutations from resistant isolates (L40F and A101E) resulted in changes in the conformational dynamics and pocket crosstalk of the individual Rv0678 monomers distinct from WT or the L40V mutation (Figure 5). In particular, A101E formed a new stable salt-bridge interaction in the "hinge" domain, which could disrupt the conformational flexibility required by this region to transition between the DNA- and ligand-bound homodimer states (Figure S4).

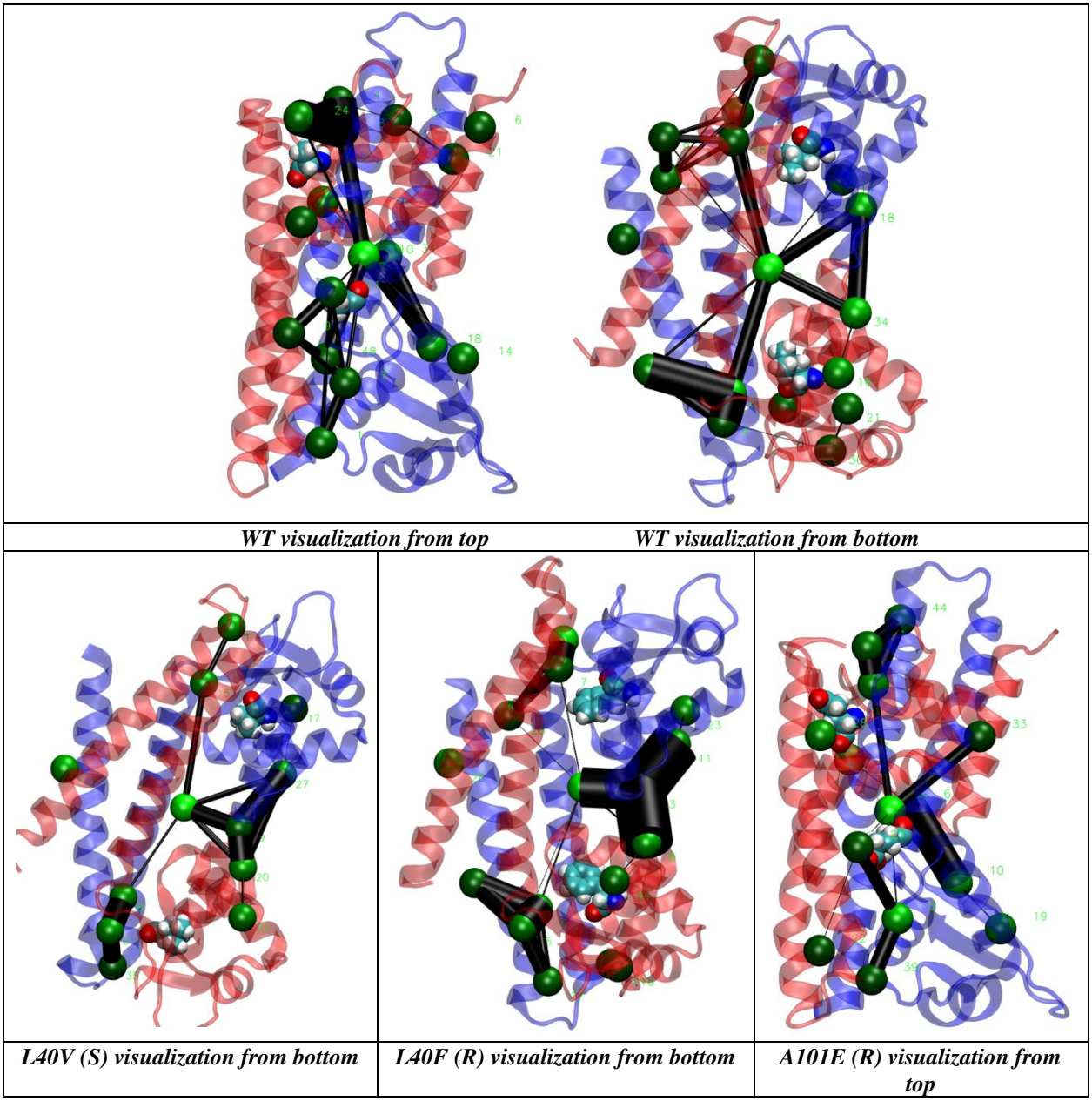

Figure 5: Networks of the most persistent pockets found in the wild-type (WT) and mutated Rv0678. The pocket crosstalk analysis on simulated systems identifies allosteric signaling. All systems shared a large common pocket located at the interface of the two monomers (Figure S5). This large pocket communicates with other smaller pockets at different zones of the homodimer by the network edges (black lines). Comparative analysis showed that the resistance-conferring mutations, L40F and A101E displayed different network edges during the 100ns of simulations with respect to the WT. R- resistant, S-susceptible

Discussion

In this study, we identify new bedaquiline and clofazimine resistance determinants by combining *in vitro* evolution experiments with WGS and MIC data, including the analysis of 14,151 clinical Mtbc strains provided by the CRyPTIC consortium (http://www.crypticproject.org/). The results have allowed us to define a comprehensive set of genomic variants associated with resistance to BDQ (& CFZ), which are central to treating MDR, pre-XDR and XDR-TB [8]. This project also demonstrates the potential of *in vitro* evolution experiments employing selection under sub-lethal drug concentrations to generate clones with a wide spectrum of mutations, including clinically relevant mutations. Collectively, this work helps extend the use of genomics in providing personalized medicine to patients with MDR, pre-XDR, and XDR-TB, through bolstering genotypic catalogues with phenotypically verified variant lists.

Although BDQ/CFZ are rolled out worldwide as core drugs in treatment regimens for MDR-TB patients [8], antibiotic susceptibility testing for these compounds is rarely available and patients are often treated empirically. Indeed, recent studies report treatment failure and/or poor outcome of MDR-TB patients as mutations in *Rv0678* emerge that are associated with BDQ/CFZ resistance [12,15,17,26,54]. Additionally, misdiagnosis can promote the selection and subsequent transmission of specific MDR Mtbc strains. For example, it was recently reported in Eswatini and South Africa, that patients infected with an MDR outbreak strain harboring the RMP mutation I491F, which is not detectable by conventional phenotypic or genotypic testing, probably continued to receive RMP although it was ineffective [30]. These strains now represent more than 60% of MDR strains in Eswatini and additionally more than half of these developed enhanced BDQ/CFZ MICs via acquired *Rv0678* mutations [1,29,30,64]. This scenario underlines the urgent need for approaches to rapidly detect resistance, including to BDQ/CFZ, with baseline diagnostics and during therapy (e.g. via WGS or targeted genome sequencing) to avoid treatment failure, further resistance development and ongoing transmission of specific MDR strains.

Genome sequencing techniques have been demonstrated to accurately identify genomic variants in all target regions involved in resistance development in a single analysis [3,65]. However, several major challenges exist—including linking genotype and phenotype to distinguish resistance-mediating from benign mutations and interpreting how multiple mutations interact when the resistance phenotype is polygenic, as is the case with BDQ and CFZ[60]. This work catalogues the phenotype of 260 unique genomic variants across six genes. Importantly, not all variation leads to resistance, as 38 of these mutations in

318 *Rv0678* are not associated with resistance to BDQ/CFZ (Table S5), which facilitates the prediction of
319 BDQ/CFZ susceptibility. Furthermore, 30/94 BDQ susceptible isolates with *Rv0678* mutations harbored an
320 additional mutation in the *mmpL5* or *mmpS5* efflux pump genes, which may abrogate the efflux pump
321 mechanism and reconstitute the susceptible phenotype[59]. Here, we provide preliminary evidence that
322 isolates with inactivating (frameshift, nonsense, or missense variants) *mmpL5* mutations can override
323 *Rv0678* resistance-mediating mutations, resulting in hyper-susceptibility to BDQ. Further work to
324 understand the frequency, distribution and origin of these inactivating mutations is necessary to
325 understand their clinical relevance worldwide.

326 While genome sequencing of clinical Mtbc strains has been deployed in several countries, its
327 implementation is constrained not just by technical and data analysis considerations, but also because
328 working directly from clinical samples (e.g. sputum) is difficult [3]. We recently demonstrated that targeted
329 genome sequencing using the commercially available Deeplex®-MycTB has a high sensitivity and
330 specificity for first- and second-line drug resistance prediction, including BDQ/CFZ resistance mutations
331 that have been found in patients [64,66,67]. In combination with our comprehensive set of mutations that
332 confer resistance to BDQ/CFZ, Deeplex®-MycTB and other targeted sequencing approaches allow for rapid
333 detection of BDQ/CFZ resistance from clinical samples in few days using small portable genome
334 sequencers such as the MinION [68].

335 Importantly, *in vitro* laboratory evolution experiments identified 50 resistance-conferring mutations that
336 have not yet appeared in clinical strains, thus allowing us to characterize and identify a significant
337 proportion of resistance-conferring mutations before they have even occurred in a patient. These results
338 highlight the value of *in vitro* evolution experiments as a complementary method for prospective
339 identification of resistance, as compared to traditional surveillance of patient isolates. Furthermore, this
340 method provides a large strain collection of *de novo* resistant clones from a comparable wild-type
341 susceptible ancestor. Finally, by using PacBio sequencing to establish the full genome sequence of mutant
342 clones without any mutations in the relevant targets, we were able to identify a large genomic inversion
343 that disrupts *Rv0678,* which should be considered as a novel BDQ/CFZ resistance mechanism.

344 Another method for prospectively identifying mutations that confer resistance is structure-based
345 modeling, which has recently been combined with machine learning methods to design algorithms for
346 predicting resistance to rifampicin, isoniazid, and pyrazinamide [69–73]. These approaches rely on the fact

that resistance-conferring mutations are often located in drug binding pockets or active sites and have distinct biophysical consequences as compared to their susceptible counterparts [74]. This study identifies several resistance mechanisms in *Rv0678* with quantifiable structural effects (protein stability, dimer interactions, SNAP2 scores, and interaction with the DNA), suggesting that a structure-based machine learning approach could also be successful for predicting BDQ/CFZ resistance.

As we have shown, any approach to predict BDQ resistance must consider not only mutations present in *Rv0678*, but also potential resistance/susceptibility determinants in other putative resistance-conferring genes e.g. *atpE*, *pepQ*, *Rv1979c,* and *mmpL/S5*. It has been attempted to predict BDQ resistance from *atpE* mutations [75], so one feasible option would be a meta-approach that flags if any individual gene-level algorithms predict resistance/susceptibility. In addition, CRyPTIC and other studies are producing large MIC datasets, which will enable much more nuanced modeling of resistance, which is particularly important for drugs with efflux-mediated resistance that often exhibit small sub-threshold changes in MIC. Although structure-based modeling is helpful in predicting resistance, these structural hypotheses must be confirmed experimentally for final validation.

As indicated by the overlap of *in vitro* selected mutations with 11 resistance conferring mutations found in patients, sub-MIC drug concentration can select for clinically relevant resistance variants. This modeling might also better imitate the intra-patient situation, since the complex pathology of TB disease prevents certain drugs (i.e. bactericidal and bacteriostatic drugs), from reaching all bacteria at a therapeutic level (for example structures like pulmonary cavities and granuloma lesions) [33,35,36,77]. BDQ and CFZ in particular do not penetrate the central caseous lesion (or necrotic center) of the granuloma effectively [34]. Although this study provides a large collection of *in vitro* selected Rv0678-mediated resistant clones, the efflux pump modulation by these various mutations was not experimentally investigated and should be explored in the future.

In addition to clear-cut resistance-associated mutations, additional “secondary” mutations were co-selected with resistance-associated variants *in vitro*. These secondary mutations affected several genes, mainly associated with cellular processes such as cell wall synthesis, metabolic processes, and protein regulation; with mutations also in genes of unknown function (Table S3). It is possible that these mutations bring about an additional phenotypic affect, or they may be compensatory mutations [5,78]. However, until

375 further experiments are conducted, such as competitive fitness assays (or even transcriptomic analysis),
376 it cannot be ruled out that these are merely hitchhiking mutations or culture-selected variants.

377 In this study, we focused on structural mechanisms of *Rv0678* mediated resistance, as these mutations
378 are the most clinically relevant and correlated with BDQ treatment failures. Other genes which have been
379 linked to BDQ or CFZ resistance, such as *atpE*, *pepQ* and *Rv1979c*, but their clinical relevance has yet to
380 be established [10,29,49,53]. In the CRyPTIC dataset we identified four *Rv1979c* variants which presented a
381 resistant phenotype to BDQ with variable CFZ cross resistance, and seven mutations in *pepQ* garnering
382 borderline BDQ resistance and variable CFZ resistance. Finally, mutations in *atpE* (coding for the target of
383 BDQ) were rare among the *in vitro* selection experiments and the CRyPTIC dataset, suggesting that *atpE*
384 mutations might have a high fitness cost.

385 In conclusion, our work advances our understanding of how resistance can arise to BDQ and CFZ. This
386 information provides an updated variant catalogue, comprising of mutations and structural variations
387 associated with BDQ/CFZ resistance as well as benign variants and mutations implicated with hyper-
388 susceptibility. Employing this information in DNA sequencing-based diagnostic approaches will allow for
389 the first time a rational design of BDQ and CFZ -containing MDR-TB therapies.

390 ## Materials and Methods

391 ### *In vitro* evolution experiments

392 *In vitro* experiments were carried out with H37Rv strain (ATCC 27294). Bedaquiline was purchased from
393 Janssen-Cilag GmbH and clofazimine was ordered from Sigma (C8895-1G) both were reconstituted from
394 powder in DMSO and stored at -20°C.

395 Evolutionary experiments were conducted with the *Mycobacterium tuberculosis* complex (Mtbc) lab strain
396 H37Rv. The bacteria were cultured from frozen stocks and (pre)cultured at 37° in 7H9 medium,
397 supplemented with 0.2% glycerol, 10% oleic albumin dextrose catalase (OADC), and 0.05% Tween^{80}
398 (termed culture medium). At exponential growth phase (between 0.3 and 0.6 optical density (OD) of
399 600nm), bacteria were transferred to new culture medium with a final OD of 0.05 in 50 mL, additionally
400 supplemented with either bedaquiline (BDQ) or clofazimine (CFZ). Four concentrations below the
401 minimum inhibitory concentration (MIC) were included for each drug at 1:2, 1:4, 1:8, and 1:16 below the

strain MIC (and an antibiotic-free control). The MIC of the susceptible WT ancestor was determined to be 0.12 mg/L BDQ and 0.5 mg/L CFZ in this culturing system.

These experiments were carried out over 20 days with five culture passages total. Culture passages were conducted every four days with a final culture OD of 0.05 transferred. After passages 1, 3, and 5; bacteria were plated on selective agar plates of 7H11, supplemented with 0.5% glycerol, 10% OADC and either 0.12 (1:2 MIC) or 0.25 (MIC) mg/L of BDQ, or 0.25 (1:2 MIC) mg/L CFZ. After 21-28 days of growth on selective agar plates, single colonies were transferred to culture medium, grown for 2-4 weeks, then two 1 mL aliquots were frozen at -80, and samples were taken for whole genome sequencing (WGS). All remaining colonies (collected by experimental condition) were collected for WGS, i.e. total population sequencing.

Whole genome sequencing

Isolates from *in vitro* evolutionary experiments underwent DNA isolation by CTAB method [79]. Paired-end DNA library preparations and sequencing was performed with Illumina technology (Nextera-XT and NextSeq500) according to the manufacturer's instructions and with a minimum average genome coverage of 50x. Fastq files (raw sequencing data) were mapped to the *M. tuberculosis* H37Rv reference genome (GenBank ID: NC_000962.3) using the MTBseq pipeline [80].

Briefly, for the analysis of single mutants we considered single nucleotide polymorphisms (SNPs) which were covered by a minimum of four reads in both forward and reverse orientation, four reads calling the allele with at least a phred score of 20, and an allele frequency of 75%. For the detection of insertions and deletion (InDels) we allowed a frequency over 50%.

Deep sequencing was conducted for population diversity analysis with an average genome wide coverage of 200 – 420; SNPs and InDels were called with at least one forward and one reverse read and a phred score >20 for at least 2 reads.

Three isolates underwent sequencing using the PacBio Sequel II System (Pacific Biosciences). Libraries were prepared with the SMRTbell® Express Template Prep Kit 2.0 according to the manufacturer's instructions. Barcoded overhang adapters for multiplexing were ordered at IDT (Integrated DNA Technologies). During demultiplexing barcodes were filtered for a minimum quality of 50t, which yielded

long read sequencing data of an average of 4.4 GB and mean subread length of 9 KB. Long read sequences were *de novo* assembled using PacBio SMRT® Link software version 9 and the "Microbial Assembly" workflow with a set genome size of 4.5 GB with default parameters.

Screening of Rv0678 mutations in clinical samples via the CRyPTIC strain collection

Patient derived Mtbc isolates were collected by CRyPTIC partners throughout 27 countries and analyzed in 14 different laboratories. Strains were selected from the CRyPTIC database for this study if they had matched genotype and phenotype data, a high quality BDQ phenotype, and a mutation in BDQ resistance associated gene (either *atpE*, *Rv1979c*, *pepQ*, *mmpL/S5*, or *Rv0678*). This led to the curation of 179 strains in total.

The full analysis pipeline for CRyPTIC is documented in [paper in preparation], but we outline the key steps here. Sequencing reads were deposited at the European Bioinformatics Institute and run through a bespoke bioinformatics pipeline (publicly available here: https://github.com/iqbal-lab-org/clockwork). In short, reads were filtered against human and other microbial species reads before being mapped to the H37Rv reference genome. Two parallel variant callers (SamTools and Cortex) were used [81,82], one of which makes high sensitivity SNP calls (SamTools) and one which makes high specificity SNP and indel calls (Cortex). A graph-based adjudication tool (Minos, https://github.com/iqbal-lab-org/minos) was then used to combine these results and create a final set of variants for downstream bioinformatics analysis. All strains were re-genotyped at positions that were variant in at least one CRyPTIC sample, creating a final variant call file with a call for each variant position in the *M. tuberculosis* H37Rv genome.

Phenotyping

In vitro single selected mutants were further analyzed for phenotypic drug susceptibility to both BDQ and CFZ by broth microtiter dilution as a resazurin assay. All mutants were grown in antibiotic free culture media to exponential growth phase (optical density of 0.3-0.8), then diluted to the McFarland standard of 1, with an additional 1:10 dilution, 100 µl of which was seeded in 96-well flat bottom plates (about $1x10^5$ CFU per well). Next 100 µL of antibiotic was added to each well with final concentrations of BDQ as follows: 8, 4, 2, 1, 0.5, 0.25, 0.12, and 0 mg/L; and CFZ: 16, 8, 4, 2, 1, 0.5, 0.25, 0.12, and 0 mg/L. Plates were sealed with permeable tape, and incubated at 37° standing, in sealed plastic boxes. After nine days incubation at 37°, 30µl of resazurin was added to each well. After overnight incubation, fluorescence and absorbance

were measure in Biotek plate reader Synergy 2. MIC was determined as the highest concentration which no bacterial growth was detected, either visually or by fluorescence measurement.

For MGIT susceptibility testing, 100µl of frozen bacterial stocks were transferred to Löwenstein-Jensen agar slants and incubated at 37° for three weeks. BACTEC™ MGIT™ 960 SIRE Kit was used and test was carried out according to manufacture instructions. Saline 0.83% solution was used for adjusting bacterial suspension concentration instead of Middlebrook 7H9 broth. Drug concentrations tested were 0.5, 1.0, and 2.0 mg/L for BDQ; 0.5, 1.0, and 2.0 mg/L for CFZ; 0.03, 0.06, and 0.12 mg/L for delamanid; and 0.5, 1.0, and 2.0 mg/L for linezolid. All MGIT tubes which were positive (growth units reached 400) before the antibiotic free growth control were considered resistant. An H37Rv WT strain was not included in this test.CRyPTIC strains were phenotyped using either the UKMYC5 plate or the updated UKMYC6 plate [83]. Plates were sealed, incubated at 37°C, and read at 14 days. In addition to manual plate readings, all plate images underwent an automated reading using AMyGDA software [46]. Plates without essential agreement for a drug MIC were marked as low quality and sent to a citizen science project (BashTheBug, http://bashthebug.net) for additional verification. Plates with exact agreement between at least two phenotyping methods were marked as high quality. Low (no method agrees) and medium (two methods with essential agreement) quality phenotypes were excluded from this analysis.

All strains included in this study had at least phenotypic data for BDQ. Some strains do not include CFZ data due to missing information, low quality analysis, or removal due to experimental error.

_Rv0678_ variant literature search

An extensive search was performed to include and summarize previously published BDQ and/or CFZ resistant associated mutations from *in vitro*, *in vivo*, and patient derived isolates. We used PubMed, Google, and Google Scholar to search literature published from 2014 to June 2021. Search criteria included the key “TB”, “Mycobacterium tuberculosis”, “MTB”, “bedaquiline”, “clofazimine”, “treatment”, “clinical report”, “patient”, “MDR-TB”, “XDR-TB”, “diarylquinoline”, and “drug resistance”.

Mutations in all resistance associated genes: *Rv0678*, *atpE*, *Rv1979c*, and *pepQ* were included in our final analysis, all variants with low MICs or multiple mutations in the same gene were excluded (Table 2, Table S5).

Structural modelling

The crystal structure of Rv0678 (PDB ID: 4NB5) was visualized using UCSF Chimera [84]. Structural alignment of the wHTH domain was performed using the MatchMaker tool in Chimera with a Needleman-Wunsch algorithm using a BLOSUM-62 matrix and was iteratively pruned until no long atom-pair was > 2 Å resulting in a final average RMSD of 0.81 Å over the 5 guide structures (PDB IDs: 5HSO, 5HSM, 4FX0, 4FX4, 4YIF). All protein stability, protein-protein and protein-DNA interactions were modeled using established mCSM methods with either ligand-bound or DNA-bound Rv0678 [85,86]. Mutations that presented both resistant and susceptible phenotypes were treated as resistant during statistical calculations. Screening our resistance catalogue for missense mutations that were resolved in the structure with phenotypes yielded 107 unique missense mutations. mCSM tools are available at http://biosig.unimelb.edu.au/biosig.

Molecular dynamics simulations

All the systems simulated in the present work, including Rv0678-WT, Rv0678-A101E, Rv0678-L40V and Rv0678-L40F, were prepared using BiKi Life Sciences Software Suite version 1.3.5 of BiKi Technologies s.r.l [87]. Each simulated system consisted of Rv0678 homodimer unit X-ray structure (PDB ID 4NB5) and the mutations were generated using UCSF Chimera software [84]. The Amber14 force field was used in all molecular dynamic simulations. TIP3P waters were added to make an orthorhombic box. Adding a suitable number of counter-ions neutralized the overall system. Then, the energy of the whole system was minimized. Four consecutive equilibration steps were then performed: 1) 100 ps in the NVT ensemble at 100K with the protein backbone restrained (k=1000 kJ/mol nm^2), 2) 100 ps in the NVT ensemble at 200K with the protein backbone similarly restrained, 3) 100 ps in the NVT ensemble at 300K with the protein backbone restrained, and 4) 1000 ps in NPT ensemble at 300K with no restraints. For atoms less than 1.1nm apart, electrostatic forces were calculated directly; for atoms further apart electrostatics were calculated using the Particle Mesh Ewald. Van der Waals forces were only calculated for atoms within 1.1 nm of one another. The temperature was held constant using the velocity rescale thermostat, which is a modification of the Berendsen's coupling algorithm. Finally, simulations 100 ns long in the NPT ensemble at 300K were performed for each system. To detect allosteric signal transmission networks across the protein surface, defined as interconnected pocket motions, we carried out the allosteric communication network analysis using the Pocketron module in BiKi Life Sciences Suite version 1.3.5 [87].

CRyPTIC Ethics statements as at 22 Feb 2021. Approval for CRyPTIC study was obtained by Taiwan Centers for Disease Control IRB No. 106209, University of KwaZulu Natal Biomedical Research Ethics Committee (UKZN BREC) (reference BE022/13) and University of Liverpool Central University Research Ethics Committees (reference 2286), Institutional Research Ethics Committee (IREC) of The Foundation for Medical Research, Mumbai (Ref nos. FMR/IEC/TB/01a/2015 and FMR/IEC/TB/01b/2015), Institutional Review Board of P.D. Hinduja Hospital and Medical Research Centre, Mumbai (Ref no. 915-15-CR [MRC]), scientific committee of the Adolfo Lutz Institute (CTC-IAL 47-J / 2017) and in the Ethics Committee (CAAE: 81452517.1.0000.0059) and Ethics Committee review by Universidad Peruana Cayetano Heredia (Lima, Peru) and LSHTM (London, UK).

Authors' contributions. LS, JC, AS, ZI, MH, KM, CU, DS, CR, KN, PF, MM and SN conceived the idea, designed the study, and analyzed and interpreted the data. All authors contributed to obtaining and assembling the data. LS, JC, AS, ZI, MM, PF and SN wrote the initial draft of the paper. All authors contributed to data interpretation, final drafting of the paper and approved the final version of the manuscript.

Competing interest. Authors declare no competing interests.

Acknowledgments. We thank Dr. Musco Giovanna and Dr. Ballabio Federico (San Raffale Hospital) for their help in the molecular dynamics set up. We would like to acknowledge the technical support at Research Center Borstel, especially Vanessa Mohr, Tanja Niemann, Carina Hahn, Silvia Mass, and Doreen Beyer for their aid in the laboratory.

Funding. All *in vitro* experimental work was financially supported though EvoLUNG: Evolutionary Medicine of the Lung, a Leibniz science campus for evolutionary medicine research (http://evolung.fz-borstel.de/). JC is funded by the Rhodes Trust and the Stanford University Medical Scientist Training program. PWF is funded by the NIHR Oxford Biomedical Research Centre, Oxford University Hospitals NHS Foundation Trust, John Radcliffe Hospital, Oxford, UK. The views expressed are those of the author(s) and not necessarily those of the NHS, the NIHR or the Department of Health. The work of the CRyPTIC consortium was supported by the Bill & Melinda Gates Foundation [OPP1133541] and the Welcome Trust [200205/Z/15/Z].

References

1. *WHO | Global tuberculosis report 2019*. http://www.who.int/tb/publications/global_report/en/ (2019).

2. Dheda, K. *et al.* The Lancet Respiratory Medicine Commission: 2019 update: epidemiology, pathogenesis, transmission, diagnosis, and management of multidrug-resistant and incurable tuberculosis. *The Lancet Respiratory Medicine* **7**, 820–826 (2019).

3. Dheda, K. *et al.* The epidemiology, pathogenesis, transmission, diagnosis, and management of multidrug-resistant, extensively drug-resistant, and incurable tuberculosis. *The Lancet Respiratory Medicine* **5**, 291–360 (2017).

4. Kendall, E. A., Fofana, M. O. & Dowdy, D. W. Burden of transmitted multidrug resistance in epidemics of tuberculosis: a transmission modelling analysis. *The Lancet Respiratory Medicine* **3**, 963–972 (2015).

5. Merker, M. *et al.* Compensatory evolution drives multidrug-resistant tuberculosis in Central Asia. *eLife* **7**, e38200 (2018).

6. Shah, N. S. *et al.* Transmission of Extensively Drug-Resistant Tuberculosis in South Africa. *New England Journal of Medicine* **376**, 243–253 (2017).

7. WHO Consolidated Guidelines on Tuberculosis, Module 4: Treatment - Drug-Resistant Tuberculosis Treatment. https://www.who.int/publications-detail-redirect/9789240007048.

8. WHO | Rapid Communication: Key changes to the treatment of drug-resistant tuberculosis. *WHO* http://www.who.int/tb/publications/2019/rapid_communications_MDR/en/.

559 9. Huitric, E. *et al.* Rates and mechanisms of resistance development in Mycobacterium tuberculosis to
560 a novel diarylquinoline ATP synthase inhibitor. *Antimicrobial Agents and Chemotherapy* (2010)
561 doi:10.1128/AAC.01611-09.

562 10. Almeida, D. *et al.* Mutations in pepQ confer low-level resistance to bedaquiline and clofazimine in
563 Mycobacterium tuberculosis. *Antimicrobial Agents and Chemotherapy* (2016)
564 doi:10.1128/AAC.00753-16.

565 11. Zhang, S. *et al.* Identification of novel mutations associated with clofazimine resistance in
566 Mycobacterium tuberculosis. *Journal of Antimicrobial Chemotherapy* (2015) doi:10.1093/jac/dkv150.

567 12. de Vos, M., Ley, S. D. & Cox, H. Bedaquiline micro-heteroresistance after tuberculosis treatment
568 cessation. *N Engl J Med* **380**, 2178–2180 (2019).

569 13. Ismail, N. A. *et al.* Defining Bedaquiline Susceptibility, Resistance, Cross-Resistance and Associated
570 Genetic Determinants: A Retrospective Cohort Study. *EBioMedicine* (2018)
571 doi:10.1016/j.ebiom.2018.01.005.

572 14. Villellas, C. *et al.* Unexpected high prevalence of resistance-associated Rv0678 variants in MDR-TB
573 patients without documented prior use of clofazimine or bedaquiline. *The Journal of antimicrobial*
574 *chemotherapy* (2017) doi:10.1093/jac/dkw502.

575 15. Kranzer, K. *et al.* New World Health Organization treatment recommendations for multidrug-resistant
576 tuberculosis: Are we well enough prepared? *American Journal of Respiratory and Critical Care*
577 *Medicine* (2019) doi:10.1164/rccm.201902-0260LE.

16. Polsfuss, S. *et al.* Emergence of Low-level Delamanid and Bedaquiline Resistance During Extremely Drug-resistant Tuberculosis Treatment. *Clinical Infectious Diseases* **69**, 1229–1231 (2019).

17. Andres, S. *et al.* Bedaquiline-Resistant Tuberculosis: Dark Clouds on the Horizon. *Am J Respir Crit Care Med* **201**, 1564–1568 (2020).

18. Islam, M. M. *et al.* Drug resistance mechanisms and novel drug targets for tuberculosis therapy. *Journal of Genetics and Genomics* **44**, 21–37 (2017).

19. Milano, A. *et al.* Azole resistance in Mycobacterium tuberculosis is mediated by the MmpS5–MmpL5 efflux system. *Tuberculosis* **89**, 84–90 (2009).

20. Radhakrishnan, A. *et al.* Crystal Structure of the Transcriptional Regulator Rv0678 of Mycobacterium tuberculosis*. *Journal of Biological Chemistry* **289**, 16526–16540 (2014).

21. Gao, Y.-R. *et al.* Structural analysis of the regulatory mechanism of MarR protein Rv2887 in M. tuberculosis. *Sci Rep* **7**, 6471 (2017).

22. Hartkoorn, R. C., Uplekar, S. & Cole, S. T. Cross-Resistance between Clofazimine and Bedaquiline through Upregulation of MmpL5 in Mycobacterium tuberculosis. *Antimicrobial Agents and Chemotherapy* **58**, 2979–2981 (2014).

23. Andries, K. *et al.* Acquired Resistance of Mycobacterium tuberculosis to Bedaquiline. *PLoS ONE* **9**, e102135 (2014).

24. Bloemberg, G. V. *et al.* Acquired Resistance to Bedaquiline and Delamanid in Therapy for Tuberculosis. *N Engl J Med* **373**, 1986–1988 (2015).

25. Hoffmann, H. *et al.* Delamanid and Bedaquiline Resistance in Mycobacterium tuberculosis Ancestral Beijing Genotype Causing Extensively Drug-Resistant Tuberculosis in a Tibetan Refugee. *Am J Respir Crit Care Med* **193**, 337–340 (2016).

26. Liu, Y. *et al.* Reduced Susceptibility of Mycobacterium tuberculosis to Bedaquiline During Antituberculosis Treatment and Its Correlation With Clinical Outcomes in China. *Clinical Infectious Diseases* (2020) doi:10.1093/cid/ciaa1002.

27. Nimmo, C. *et al.* Dynamics of within-host Mycobacterium tuberculosis diversity and heteroresistance during treatment. *EBioMedicine* **55**, (2020).

28. Xu, J. *et al.* Primary Clofazimine and Bedaquiline Resistance among Isolates from Patients with Multidrug-Resistant Tuberculosis. *Antimicrob Agents Chemother* **61**, e00239-17, e00239-17 (2017).

29. Nimmo, C. *et al.* Population-level emergence of bedaquiline and clofazimine resistance-associated variants among patients with drug-resistant tuberculosis in southern Africa: a phenotypic and phylogenetic analysis. *The Lancet Microbe* **1**, e165–e174 (2020).

30. Beckert, P. *et al.* MDR M. tuberculosis outbreak clone in Eswatini missed by Xpert has elevated bedaquiline resistance dated to the pre-treatment era. *Genome Medicine* **12**, 104 (2020).

31. Liu, A. *et al.* Selective Advantage of Resistant Strains at Trace Levels of Antibiotics: a Simple and Ultrasensitive Color Test for Detection of Antibiotics and Genotoxic Agents. *Antimicrobial Agents and Chemotherapy* **55**, 1204–1210 (2011).

32. Gullberg, E. *et al.* Selection of Resistant Bacteria at Very Low Antibiotic Concentrations. *PLoS Pathogens* **7**, e1002158 (2011).

33. Dartois, V. The path of anti-tuberculosis drugs: from blood to lesions to mycobacterial cells. *Nat Rev Micro* **12**, 159–167 (2014).

34. Sarathy, J. P. *et al.* Prediction of Drug Penetration in Tuberculosis Lesions. *ACS Infect Dis* **2**, 552–563 (2016).

35. Prideaux, B. *et al.* The association between sterilizing activity and drug distribution into tuberculosis lesions. *Nature Medicine* (2015) doi:10.1038/nm.3937.

36. Dheda, K. *et al.* Drug-penetration gradients associated with acquired drug resistance in patients with tuberculosis. *American Journal of Respiratory and Critical Care Medicine* (2018) doi:10.1164/rccm.201711-2333OC.

37. Cicchese, J. M., Dartois, V., Kirschner, D. E. & Linderman, J. J. Both Pharmacokinetic Variability and Granuloma Heterogeneity Impact the Ability of the First-Line Antibiotics to Sterilize Tuberculosis Granulomas. *Front. Pharmacol.* **11**, (2020).

38. Strydom, N. *et al.* Tuberculosis drugs' distribution and emergence of resistance in patient's lung lesions: A mechanistic model and tool for regimen and dose optimization. *PLOS Medicine* **16**, e1002773 (2019).

39. Greenwood, D. J. *et al.* Subcellular antibiotic visualization reveals a dynamic drug reservoir in infected macrophages. *Science* **364**, 1279–1282 (2019).

40. Fearns, A., Greenwood, D. J., Rodgers, A., Jiang, H. & Gutierrez, M. G. Correlative light electron ion microscopy reveals in vivo localisation of bedaquiline in Mycobacterium tuberculosis–infected lungs. *PLOS Biology* **18**, e3000879 (2020).

637 41. Kadura, S. *et al.* Systematic review of mutations associated with resistance to the new and repurposed
638 Mycobacterium tuberculosis drugs bedaquiline, clofazimine, linezolid, delamanid and pretomanid.
639 *Journal of Antimicrobial Chemotherapy* **75**, 2031–2043 (2020).

640 42. Song, H., Sandie, R., Wang, Y., Andrade-Navarro, M. A. & Niederweis, M. Identification of outer
641 membrane proteins of Mycobacterium tuberculosis. *Tuberculosis* **88**, 526–544 (2008).

642 43. Gu, S. *et al.* Comprehensive Proteomic Profiling of the Membrane Constituents of a Mycobacterium
643 tuberculosis Strain*S. *Molecular & Cellular Proteomics* **2**, 1284–1296 (2003).

644 44. Hunt, M. *et al.* ARIBA: rapid antimicrobial resistance genotyping directly from sequencing reads.
645 *Microbial Genomics,* **3**, e000131 (2017).

646 45. WHO | Technical report on critical concentrations for TB drug susceptibility testing of medicines used
647 in the treatment of drug-resistant TB. *WHO*
648 http://www.who.int/tb/publications/2018/WHO_technical_report_concentrations_TB_drug_susce
649 ptibility/en/.

650 46. Fowler, P. W. *et al.* Automated detection of bacterial growth on 96-well plates for high-throughput
651 drug susceptibility testing of mycobacterium tuberculosis. *Microbiology (United Kingdom)* (2018)
652 doi:10.1099/mic.0.000733.

653 47. Kaniga, K. *et al.* A Multilaboratory, Multicountry Study To Determine Bedaquiline MIC Quality Control
654 Ranges for Phenotypic Drug Susceptibility Testing. *J Clin Microbiol* **54**, 2956–2962 (2016).

655 48. Schön, T. *et al.* Wild-type distributions of seven oral second-line drugs against Mycobacterium
656 tuberculosis. *Int J Tuberc Lung Dis* **15**, 502–509 (2011).

49. Veziris, N. *et al.* Rapid emergence of Mycobacterium tuberculosis bedaquiline resistance: lessons to avoid repeating past errors. *Eur Respir J* **49**, 1601719 (2017).

50. Battaglia, S. *et al.* Characterization of Genomic Variants Associated with Resistance to Bedaquiline and Delamanid in Naive Mycobacterium tuberculosis Clinical Strains. *J Clin Microbiol* **58**, (2020).

51. Zimenkov, D. V. *et al.* Examination of bedaquiline- and linezolid-resistant Mycobacterium tuberculosis isolates from the Moscow region. *Journal of Antimicrobial Chemotherapy* **72**, 1901–1906 (2017).

52. Yang, J. S., Kim, K. J., Choi, H. & Lee, S. H. Delamanid, Bedaquiline, and Linezolid Minimum Inhibitory Concentration Distributions and Resistance-related Gene Mutations in Multidrug-resistant and Extensively Drug-resistant Tuberculosis in Korea. *Ann Lab Med* **38**, 563–568 (2018).

53. Ghodousi, A. *et al.* Acquisition of Cross-Resistance to Bedaquiline and Clofazimine following Treatment for Tuberculosis in Pakistan. *Antimicrob Agents Chemother* **63**, e00915-19, /aac/63/9/AAC.00915-19.atom (2019).

54. Nimmo, C. *et al.* Bedaquiline resistance in drug-resistant tuberculosis HIV co-infected patients. *European Respiratory Journal* (2020) doi:10.1183/13993003.02383-2019.

55. Wang, G. *et al.* Prevalence and molecular characterizations of seven additional drug resistance among multidrug-resistant tuberculosis in China: A subsequent study of a national survey. *J Infect* **82**, 371–377 (2021).

56. Xu, J. *et al.* Verapamil Increases the Bioavailability and Efficacy of Bedaquiline but Not Clofazimine in a Murine Model of Tuberculosis. *Antimicrobial Agents and Chemotherapy* **62**, e01692-17.

57. Pang, Y. *et al.* In Vitro Drug Susceptibility of Bedaquiline, Delamanid, Linezolid, Clofazimine, Moxifloxacin, and Gatifloxacin against Extensively Drug-Resistant Tuberculosis in Beijing, China. *Antimicrob Agents Chemother* **61**, e00900-17, e00900-17 (2017).

58. Consortium, T. Cr. & Fowler, P. W. Epidemiological cutoff values for a 96-well broth microdilution plate for high-throughput research antibiotic susceptibility testing of M. tuberculosis. *medRxiv* 2021.02.24.21252386 (2021) doi:10.1101/2021.02.24.21252386.

59. Vargas, R. *et al.* The role of epistasis in amikacin, kanamycin, bedaquiline, and clofazimine resistance in Mycobacterium tuberculosis complex. *bioRxiv* 2021.05.07.443178 (2021) doi:10.1101/2021.05.07.443178.

60. Merker, M. *et al.* Phylogenetically informative mutations in genes implicated in antibiotic resistance in Mycobacterium tuberculosis complex. *Genome Med* **12**, 27 (2020).

61. Hecht, M., Bromberg, Y. & Rost, B. Better prediction of functional effects for sequence variants. *BMC Genomics* **16**, S1 (2015).

62. Kumarevel, T. The MarR Family of Transcriptional Regulators - A Structural Perspective. *Antibiotic Resistant Bacteria - A Continuous Challenge in the New Millennium* (2012) doi:10.5772/28565.

63. Hong, M., Fuangthong, M., Helmann, J. D. & Brennan, R. G. Structure of an OhrR-ohrA operator complex reveals the DNA binding mechanism of the MarR family. *Molecular Cell* (2005) doi:10.1016/j.molcel.2005.09.013.

64. Makhado, N. A. *et al.* Outbreak of multidrug-resistant tuberculosis in South Africa undetected by WHO-endorsed commercial tests: an observational study. *The Lancet Infectious Diseases* **18**, 1350–1359 (2018).

65. Gröschel, M. I. *et al.* Pathogen-based precision medicine for drug-resistant tuberculosis. *PLoS Pathog* **14**, e1007297 (2018).

66. Feuerriegel, S. *et al.* Rapid genomic first- and second-line drug resistance prediction from clinical Mycobacterium tuberculosis specimens using Deeplex®-MycTB. *European Respiratory Journal* (2020) doi:10.1183/13993003.01796-2020.

67. Jouet, A. *et al.* Deep amplicon sequencing for culture-free prediction of susceptibility or resistance to 13 anti-tuberculous drugs. *European Respiratory Journal* (2020) doi:10.1183/13993003.02338-2020.

68. Cabibbe, A. M. *et al.* Application of Targeted Next-Generation Sequencing Assay on a Portable Sequencing Platform for Culture-Free Detection of Drug-Resistant Tuberculosis from Clinical Samples. *Journal of Clinical Microbiology* **58**, (2020).

69. Kumar, S. & Jena, L. Understanding Rifampicin Resistance in Tuberculosis through a Computational Approach. *Genomics Inform* **12**, 276–282 (2014).

70. Zhang, Q. *et al.* Uncovering the Resistance Mechanism of Mycobacterium tuberculosis to Rifampicin Due to RNA Polymerase H451D/Y/R Mutations From Computational Perspective. *Front. Chem.* **7**, (2019).

712 71. Marney, M. W., Metzger, R. P., Hecht, D. & Valafar, F. Modeling the structural origins of drug
713 resistance to isoniazid via key mutations in Mycobacterium tuberculosis catalase-peroxidase, KatG.
714 *Tuberculosis* **108**, 155–162 (2018).

715 72. Mehmood, A. *et al.* Structural Dynamics Behind Clinical Mutants of PncA-Asp12Ala, Pro54Leu, and
716 His57Pro of Mycobacterium tuberculosis Associated With Pyrazinamide Resistance. *Front. Bioeng.*
717 *Biotechnol.* **7**, (2019).

718 73. Carter, J. J. *et al.* Prediction of pyrazinamide resistance in Mycobacterium tuberculosis using
719 structure-based machine learning approaches. *bioRxiv* 518142 (2019) doi:10.1101/518142.

720 74. Tunstall, T. *et al.* Combining structure and genomics to understand antimicrobial resistance.
721 *Computational and Structural Biotechnology Journal* **18**, 3377–3394 (2020).

722 75. Karmakar, M. *et al.* Empirical ways to identify novel Bedaquiline resistance mutations in AtpE. *PLOS*
723 *ONE* **14**, e0217169 (2019).

724 76. Dartois, V. The path of anti-tuberculosis drugs: From blood to lesions to mycobacterial cells. *Nature*
725 *Reviews Microbiology* (2014) doi:10.1038/nrmicro3200.

726 77. Strydom, N. *et al.* Tuberculosis drugs' distribution and emergence of resistance in patient's lung
727 lesions: A mechanistic model and tool for regimen and dose optimization. *PLoS Medicine* (2019)
728 doi:10.1371/journal.pmed.1002773.

729 78. Müller, B., Borrell, S., Rose, G. & Gagneux, S. The heterogeneous evolution of multidrug-resistant
730 Mycobacterium tuberculosis. *Trends in Genetics* **29**, 160–169 (2013).

79. van Soolingen, D., Hermans, P. W., de Haas, P. E., Soll, D. R. & van Embden, J. D. Occurrence and stability of insertion sequences in Mycobacterium tuberculosis complex strains: evaluation of an insertion sequence-dependent DNA polymorphism as a tool in the epidemiology of tuberculosis. *Journal of Clinical Microbiology* **29**, 2578–2586 (1991).

80. Kohl, T. A. *et al.* MTBseq: a comprehensive pipeline for whole genome sequence analysis of Mycobacterium tuberculosis complex isolates. *PeerJ* **6**, e5895 (2018).

81. Li, H. *et al.* The Sequence Alignment/Map format and SAMtools. *Bioinformatics* **25**, 2078–2079 (2009).

82. Iqbal, Z., Caccamo, M., Turner, I., Flicek, P. & McVean, G. De novo assembly and genotyping of variants using colored de Bruijn graphs. *Nature Genetics* **44**, 226–232 (2012).

83. Rancoita, P. M. V. *et al.* Validating a 14-Drug Microtiter Plate Containing Bedaquiline and Delamanid for Large-Scale Research Susceptibility Testing of Mycobacterium tuberculosis. *Antimicrob Agents Chemother* **62**, e00344-18, /aac/62/9/e00344-18.atom (2018).

84. Pettersen, E. F. *et al.* UCSF Chimera—A visualization system for exploratory research and analysis. *Journal of Computational Chemistry* **25**, 1605–1612 (2004).

85. Pires, D. E. V., Blundell, T. L. & Ascher, D. B. MCSM-lig: Quantifying the effects of mutations on protein-small molecule affinity in genetic disease and emergence of drug resistance. *Scientific Reports* **6**, 1–8 (2016).

86. Pires, D. E. V., Ascher, D. B. & Blundell, T. L. MCSM: Predicting the effects of mutations in proteins using graph-based signatures. *Bioinformatics* **30**, 335–342 (2014).

87. Decherchi, S., Bottegoni, G., Spitaleri, A., Rocchia, W. & Cavalli, A. BiKi Life Sciences: A New Suite for Molecular Dynamics and Related Methods in Drug Discovery. *J. Chem. Inf. Model.* **58**, 219–224 (2018).